International Journal of Environmental Sciences
ISSN: 2229-7359
Vol. 11 No. 8, 2025
https://www.theaspd.com/ijes.php

Analysis Of Solar PV Array Under Abnormal Grid Anomalies Using Intelligent Control Strategies

G. Shree Prudhvi[1], P. Bharat Kumar[2], P. Sujatha[3]
[1]PG-Scholar, Department of EEE, JNTUA College of Engineering (Autonomous) Ananthapuramu, India. gshrip1107@gmail.com
[2]Assistant Professor, Department of EEE, JNTUA College of Engineering (Autonomous) Ananthapuramu, India. pbk.eee@jntua.ac.in
[3]Professor, Department of EEE, JNTUA College of Engineering (Autonomous) Ananthapuramu, India. psujatha.eee@jntua.ac.in

Abstract
This paper investigates a grid-connected solar photovoltaic (PV) array system under linear and non-linear load conditions, focusing on advanced control techniques to enhance power quality. Initial evaluations under abnormal grid conditions reveal significant levels of Total Harmonic Distortion (THD) in grid voltage and current. To address this issue, the study explores the application of Artificial Neural Network (ANN) and Fuzzy Logic Controllers (FLC). In the first approach, an ANN controller is employed, resulting in a noticeable reduction in THD. In the second approach, a combination of an ANN controller and a Fuzzy Logic Controller achieves even greater improvements in harmonic performance. This work highlights the effectiveness of intelligent control strategies, such as ANN and Fuzzy Logic, in reducing harmonics in solar PV systems. The findings contribute to the advancement of reliable and power-efficient grid-connected solar PV systems.
Keywords: *Solar Photovoltaic System, Maximum Power Point Tracking, Total Harmonic Distortion (THD), Artificial Neural Network (ANN), Fuzzy Logic Controller (FLC).*

1. INTRODUCTION

As energy demands continue to grow and environmental concerns escalate, photovoltaic (PV) systems have emerged as a key solution for sustainable power generation [7]. These systems rely on clean and renewable energy sources, offering a significant reduction in emissions of greenhouse gases in comparison to conventional power generation techniques [1], [9]. Grid-connected PV systems are widely utilized across industries and are designed to operate effectively under various load conditions, including both linear and non-linear loads [18]. However, their performance can be adversely affected by factors such as grid disturbances, harmonic distortion, and the inherent non-linear behaviour of PV modules [16].

Given the variability in power generation caused by fluctuations in solar irradiance and temperature, Maximizing energy output demands that High Power Point Tracking be used or MPPT, algorithms [20]. This study utilizes the Incremental Conductance (INC) technique for MPPT due to its capability to adapt to rapidly changing environmental conditions and ensure efficient energy harvesting [22]. Advanced control techniques were used to further address grid voltage and current Total Harmonic Distortion (THD). Artificial Neural Networks (ANN) were integrated into the MPPT process, and their application, alongside adaptive and fuzzy logic controllers in the Voltage Source Converter (VSC), significantly enhanced system performance [3], [5].

These intelligent control strategies effectively reduced harmonic distortion and improved overall power quality [4], [21]. This research highlights the effectiveness of combining the INC-based MPPT approach with ANN and fuzzy logic controllers to minimize harmonics, enhance system efficiency, and guarantee steady operation with different grid and load situations. [10], [13]. The findings contribute to the development of reliable and high-performance grid-connected PV systems [14], [24].

2. SYSTEM DESCRIPTION

The Figure. 1 provides a visual representation of the system architecture. The boost converter is connected to the PV array, VSC, and the grid through clearly marked paths. The figure highlights key components, including the passive filter, control mechanisms, and load representations, illustrating the system's integrated design for efficient renewable energy application [15].

The solar photovoltaic (PV) system integrates a PV array with a three-phase grid to ensure efficient energy generation, conversion, and grid synchronization [11]. The PV array runs at its highest power level (MPP) of 270V and 18A, supported by glass insulation with a thickness of 2.5 mm and a relative permittivity of 6 for electrical safety and durability [2].The generated DC power is stepped up using a boost converter equipped with a 5 mH inductor to match the required grid voltage level. A 5 mF DC-link capacitor stabilizes the voltage and provides transient support during dynamic operations [13]. Using a Voltage Source Conversion (VSC), the system transforms the processed DC electricity into AC. The VSC makes sure the power produced matches with the grid's voltage and frequency, enabling seamless synchronization [18]. To suppress harmonics and improve power quality, a passive filter consisting of a 1.25 kΩ resistance and a 125 nF capacitance is integrated into the system [14], [15]. The grid connection also features an interfacing inductor (8 mH) and grid impedance (0.1 mH inductance and 20 mΩ resistance) to manage power flow and transients effectively [26].The system incorporates advanced Maximum Power Point Tracking (MPPT) functionality using the Incremental Conductance (INC) algorithm [20]. This algorithm dynamically adjusts the operating PV array voltage by contrasting the incremental conductance (dI_{pv}/dV_{pv}) with the instantaneous conductance (I_{pv}/V_{pv}). This adjustment ensures optimal power extraction even being exposed to several environmental factors, including variations in temperature and sun irradiance [21].

Figure 1 Block Diagram of Grid-Connected Solar PV System.

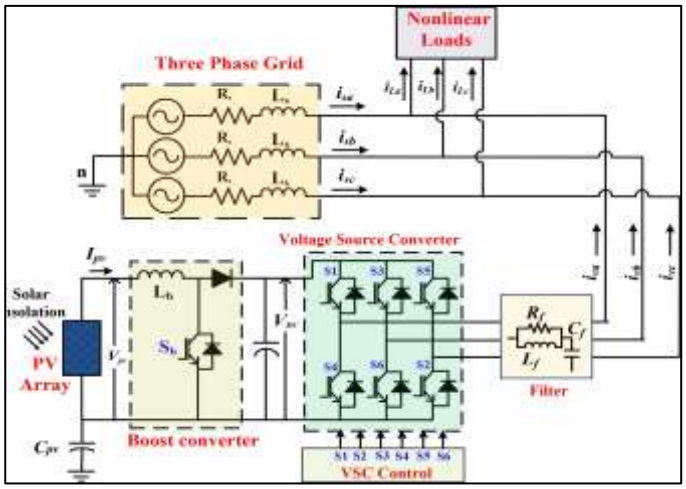

After being transformed into AC, energy is then supplied into the grid. The passive filter minimizes Total Harmonic Distortion (THD), ensuring high power quality and compliance with grid standards [16]. The system also includes a representation of practical load conditions using a Resistance load (120 Ω) and inductive load in a diode bridge rectifier (100 mH) [19]. High-frequency sampling, with a 30 µs sampling time, facilitates precise real-time monitoring and control, ensuring the system adapts efficiently to changes in load and grid conditions [27].

The integrated design of the system ensures reliable and efficient operation, delivering clean energy to the grid while maintaining power quality. This setup demonstrates its capability to meet the demands of renewable energy applications, handling both linear and non-linear loads effectively[23].

3. FILTER DESIGN

The Figure. 2 presents the schematic of the proposed passive filter [1], It is intended to reduce the harmonics of voltage and current caused by shifting in an electrical conversion. The filter consists of a resistor (R_f), inductor (L_f), and capacitor (C_f) arranged in both series and parallel configurations.

This arrangement allows the filter to suppress harmonics effectively, improving the system's overall performance and ensuring smoother operation. The filter's characteristics are represented by a transfer function of the second order. The filter's input impedance (Z_{in}) plays a crucial role in determining its effectiveness in harmonic suppression, and its mathematical expression provides a comprehensive understanding of the filter's behavior. By carefully selecting the values of R_f, L_f, and C_f, the filter is optimized for enhanced functionality in the system.

Figure 2 Filter Design

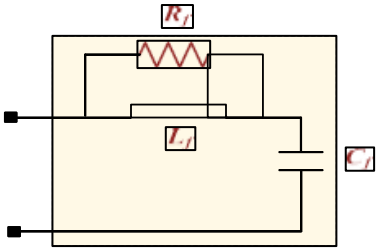

The input impedance is expressed as,

$$Z_{in} = \frac{sR_f L_f}{R_f + sL_f} + \frac{1}{sC_f}$$

The above equation is expressed by rearranging the several terms as,

$$Z_{in} = \frac{\frac{s^2}{1/L_f C_f} + \frac{s}{R_f/L_f} + 1}{(sC_f)\left(1 + \frac{s}{R_f/L_f}\right)}$$

This passive filter design is essential for suppressing voltage and current harmonics generated by switching in a voltage source converter.

The combination of R_f, L_f, and C_f allows effective harmonic reduction, ensuring smoother and more stable operation of the system. The input impedance (Z_{in}) provides a mathematical basis for analyzing the filter's performance and understanding its behavior.

4. CONTROL STRATEGIES

4.1 ADAPTIVE CONTROLLER

The grid-side network may be impacted by variations in the a number of nonlinear and linear loads that are coupled at the connection point, as seen in Fig. 1. To improve the performance of the system, precisely estimating The fundamental load current component is necessary. The whole strategy is broken down into two sections: (1) basic (2) basic load component estimate, and (3) load current modelling. The precise steps are as follows:

1) Fundamental Load Current Modelling: The load current (i_L) consists of a fundamental component and various harmonic components. It can be expressed as:

$$i_L = I_{L1} \sin(\omega_1 t + \varphi_1) + I_{L3} \sin(\omega_3 t + \varphi_3) + \ldots + I_{Ln} \sin(\omega_n t + \varphi_n) \quad (1)$$

where I_{Ln}, φ_n, and ω_n represent the nth harmonic component's angular frequency, phase, and amplitude, in that order. A low-pass filter (U(s)) is used to channel the load current in order to eliminate high-frequency noise. leading to the filtered current (x), which is provided by:

$$x = U(s)\, i_L \quad (2)$$

If the known and unknown terms can be separated within the given matrix representation, the vector can be classified as linearly parameterizableq. Using a linear parametric model transformation [4], [5], [6], Both the fundamental and harmonics components of the load current can be used to express it.

$$i_L = [I_{L11} I_{L12} \ldots\ldots I_{Ln1} I_{Ln2}] \begin{bmatrix} \sin \omega_1 t \\ \cos \omega_1 t \\ \ldots\ldots \\ \ldots\ldots \\ \sin \omega_n t \\ \cos \omega_n t \end{bmatrix} \quad (3)$$

Where $I_{Ln1} = I_{Ln} \sin \varphi_n$, $I_{Ln2} = I_{Ln} \cos \varphi_n$. In (1) equation, the The quadrature and in-phase components are rearranged as

$$x = U(s)\, \theta^{*T} \emptyset \quad (4)$$

$$\theta^{*T} = [I_{L11}, I_{L12}, I_{L31}, I_{L32}, \ldots\ldots, I_{LN1}, I_{LN2}]^T \quad (5)$$

$$\emptyset = [\sin \omega_1 t, \cos \omega_1 t, \ldots\ldots, \sin \omega_n t, \cos \omega_n t] \quad (6)$$

where x, θ^*, and $\emptyset$ represent the recognised components, unknown parameters, and post-filtered current component, in that order. The unknown parameter's estimation ($\hat{\theta}$) is formulated as below to determine the system behaviour.

$$\hat{\theta} = [\hat{I}_{L11}, \hat{I}_{L21}, \hat{I}_{L31}, \hat{I}_{L32}, \ldots\ldots, \hat{I}_{Ln1}, \hat{I}_{Ln2}]^T \quad (7)$$

Using the amplitudes of the desired signal's in-phase and quadrature components, the nth harmonic's amplitude and phase are calculated. providing a clear representation of the harmonic characteristics.

2) Fundamental Load Component Estimation: The estimate of the error (h) is employed to determine the load current's basic load component. represented in a simplified form as:

$$h = -U\tilde{\theta}\emptyset \quad (8)$$

where $\tilde{\theta} = \theta - \theta^*$, $\emptyset \in l_\infty$. The integral cost function (J(θ)) [5], [6], is defined with ϑ as a forgetting factor,

$$J(\theta) = \frac{1}{2}\int_0^t e^{-\vartheta(t-\tau)} h^2(t,\tau)d\tau \quad (9)$$

$$h(t,\tau) = x(\tau) - \theta^T(t)\emptyset(t)/m^2(\tau) \quad (10)$$

which ensures that the influence of past data $\tau < 1$ diminishes exponentially over time. Consequently, the estimated parameter trajectory, ($\theta(t)$), is updated continually to reduce the integral price function according to all historical data. The unidentified parameters (θ) are calculated by minimising the integral rectangular of the transient error, as described in equation (9).

$$J(\theta) = \left(\frac{1}{2}\right)\int_0^t e^{-\vartheta(t-\tau)}\left(\frac{x(\tau)}{m^2(\tau)} - \frac{\theta^T(t)\emptyset(t)}{m^2(\tau)}\right)d\tau \quad (11)$$

Notably, the whole cost function $J(\theta)$ is convex in the parameter space θ, simplifying the optimization process. A first-order iterative optimization method is employed to reduce J(θ) in relation to θ.

$$\dot{\boldsymbol{\theta}} = -\boldsymbol{\Gamma}\boldsymbol{\Delta J} = -\boldsymbol{\Gamma}\int_0^t \boldsymbol{e^{-\vartheta(t-\tau)}}\left(\frac{\boldsymbol{x(\tau)}}{\boldsymbol{m^2(\tau)}} - \frac{\boldsymbol{\theta^T(t)\emptyset(t)}}{\boldsymbol{m^2(\tau)}}\right)\boldsymbol{d\tau} \quad (12)$$

Here, Γ > 0 represents the adaptive gain used in the optimization. Basic and harmonic component estimation adaptive rules guarantee that $\emptyset/m$ is bounded,

$$\dot{\boldsymbol{\theta}} = -\boldsymbol{\Gamma}(\boldsymbol{N(t)\theta} + \boldsymbol{C(t)}) \quad (13)$$

$$\dot{\boldsymbol{N}} = -\vartheta N + \frac{\emptyset\emptyset^T}{\boldsymbol{m^2}} \quad (14)$$

$$\dot{\boldsymbol{C}} = -\boldsymbol{\vartheta}C + \frac{\boldsymbol{x\emptyset}}{\boldsymbol{m^2}} \quad (15)$$

making the parameters N and C inherently bounded as well. This guarantees stability and accurate estimation of the desired components.

4.2 ANN CONTROLLER

The ANN plays a critical role in optimizing the performance of the PV-grid energy conversion system. By mimicking the learning and decision-making capabilities of the human brain, the ANN efficiently handles complex, linear, and non-linear challenges. It is particularly used to regulate the The algorithm known as maximum point tracking (MPPT), ensuring optimal power extraction under varying conditions.

Figure 3 ANN Structure.

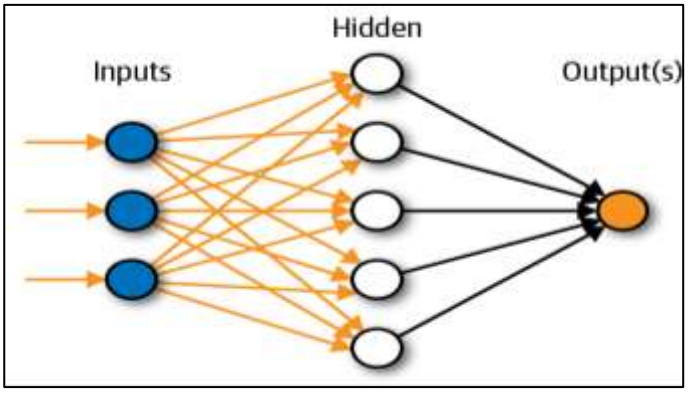

Structure and Features

- Network-Architecture

The ANN is designed as a double-layer feed-forward neural network. This architecture ensures data flows in a single direction (input to output) without feedback loops, making it suitable for real-time applications like MPPT control.

- Input Layer

o The input layer contains 1 neuron that processes the reference voltage.

o This reference voltage represents the desired operating point for extracting maximum power from the PV system.

- Hidden Layer

o The network includes a single hidden layer with 20 neurons.

o Each neuron The hyperbolic tang sigmoid activation function, which transfers the inputs to a range of -1 to 1, is used in the hidden layer.

o This transfer function helps the network identify non-linear relationships between the input and the output, making it effective in adapting to system anomalies.

- Output Layer

o The output layer consists of 20 neurons, each associated with one control signal.

o A positive linear activation function is applied, ensuring the output signals remain proportional to the processed input data.

- Bias and Weights

o The bias values for the hidden and output layers consist of 20 reference voltage values. These bias values act as thresholds for activating neurons.

o Weights determine the influence of input signals on each neuron and are adjusted during the training phase to minimize errors.

- Training Algorithm

o The network is trained using the Levenberg-Marquardt algorithm, a robust optimization technique.This algorithm iteratively updates weights and biases to reduce the discrepancy between the intended control signal and the expected output.

o The algorithm is chosen for its efficiency and faster convergence during training, ensuring the network is ready for real-time control.

Functioning

- Input Data Collection

o Sensors in the PV system measure real-time parameters like reference voltage, representing the system's operational circumstances.

o This data is fed to the ANN's input layer for processing.

- Processing Through the Hidden Layer

o The hidden layer receives the input signal, and each neuron performs a weighted summation of the input data and adds a bias.

o The hyperbolic tangent sigmoid activation function is applied to these summations to identify and model non-linear relationships. This step is crucial for adapting to dynamic environmental changes such as fluctuations in solar irradiance or temperature.

- Training Phase

o During the network's development, it is trained using a dataset containing historical input-output pairs.

o The Levenberg-Marquardt algorithm is employed to optimize weights and biases, reducing the discrepancy between the intended outputs and the network's predictions.

o Once trained, the ANN can generalize its learned behavior to new, unseen scenarios.

- Output Generation

o The processed signals sent to the final result layer from the concealed layer.

o Here, the positive linear activation function ensures the control signals are proportional to the refined input data.

o These control signals are then used to regulate the MPPT algorithm, ensuring maximum power extraction and system stability.

4.3 FUZZY LOGIC CONTROLLER DESIGN

In a connected to the grid solar PV array, the Power Source Converter (VSC) is managed by the Fuzzy Logic The controller (FLC). An error but Change in Error are used as inputs, and a control is produced. signal as an output to ensure optimal operation of the VSC.

Fuzzification:

Membership functions are used to transform clear (numerical) values provided into fuzzy sets. In this system:

Inputs:

1. Error (e): The variation between the voltage of the reference and the voltage of the voltage source converter (VSC).
2. Error Change (Δe): The error signal's rate of change over time.

Membership Functions:

The fuzzy sets for both inputs are defined using triangular membership functions:

- NB (Negative Big): Represents a significant negative value.
- NM (Negative Medium): Represents a medium negative value.
- NS (Negative Small): Represents a small negative value.
- ZE (Zero): Represents a near-zero value.
- PS (Positive Small): Represents a small positive value.
- PM (Positive Medium): Represents a medium positive value.
- PB (Positive Big): Represents a large positive value.

Rule Base:

The rule base is made up of a series of IF-THEN constraints that specify how inputs (error and error change) and the outcome (control signal) relate to one another. For the Mamdani fuzzy interface system [3], the rules are typically heuristic. The link of both inputs and outcomes in an arrangement of fuzzy logic is represented by rules that are described using linguistic concepts. A rule might say, for instance:

If the error code is NB and the error change is NM, the output will also be NB.

This rule leverage the fuzzified inputs to determine the corresponding fuzzy set for the output, which represents the control signal. This approach ensures that the system's behavior is intuitive and adaptable to varying conditions.

Rule Implementation:

The rules are implemented in a tabular form (Table-I) to facilitate computation and ensure systematic coverage of all possible input combinations. The Mamdani FIS uses the rule base during inference to evaluate the fuzzy inputs, apply the logical operators (e.g., AND, OR), and produce the fuzzy output, which is later de-fuzzified into a crisp control signal.

Table 1 Decision Table

Error/Change in Error	NB	NM	NS	ZE	PS	PM	PB
NB	NB	NB	NM	NM	NS	ZE	PS
NM	NB	NM	NM	NS	ZE	PS	PM
NS	NM	NM	NS	ZE	PS	PM	PM
ZE	NM	NS	ZE	ZE	ZE	PS	PM
PS	NS	ZE	PS	ZE	PS	PM	PB
PM	ZE	PS	PS	PM	PM	PB	PB
PB	PS	PS	PM	PB	PB	PB	PB

Defuzzification:

Defuzzification is how the final control step is determined by turning the combined fuzzy result into a precise value. The centroid approach, which determines the weighed mean of the fuzzy output, is frequently employed for this purpose. The formula for the centroid method is:

$$y_{defuzzified} = \frac{\sum \mu(y).y}{\sum \mu(y)}$$

Here, $\mu(y)$ represents the membership value at a specific output point y, and y denotes the output value. This method ensures that The fuzzy set's centre of gravity is reflected in the clear output, providing a single value for the control signal.

Dataset:

The dataset required for this system includes values of Error (e), which is the rate at which the error signal changes, and the shift, in Error (Δe), where is the deviation between the voltage that serves as the reference and the actual voltage. Included in the output dataset are control signals generated to adjust the Voltage Source Converter (VSC) effectively based on the input conditions.

The inference mechanism in the Mamdani fuzzy inference system involves key steps. First, the crisp inputs, such as Error and Change in Error, are fuzzified into their corresponding fuzzy sets based on predefined membership functions. Next, the appropriate rules are activated based on these fuzzified inputs. As a case in point, if the mistake is made and its change belong to certain linguistic categories, the corresponding rules that link these inputs to an output are triggered. Multiple rules may be activated simultaneously, each contributing a fuzzy output. Finally, the fuzzy outputs from all activated rules are aggregated using methods like max-min composition to form a combined fuzzy output, which represents the system's response.

5. TOTAL HARMONIC DISTORTION (THD)

Total harmony distortion (THD) is a crucial factor in determining how well the solar PV system is supplying the grid with power. When integrating the PV system's DC output with the AC grid, the Voltage Source Converter (VSC) produces switching harmonics that have the potential to skew the grid current waveform. In order to guarantee adherence to power quality regulations and dependable grid functioning, the THD needs to be reduced. THD is a measure of how much the grid current deviates from an ideal sinusoidal waveform due to the presence of harmonics, which are unwanted frequencies that are multiples of the basic grid frequency in whole numbers. A lower THD indicates that the grid current is closer to a pure sinusoidal wave, ensuring better power quality. The THD in the system is calculated using the formula:

$$\text{THD}\% = \frac{\sqrt{V_2^2 + V_3^2 + \cdots\ldots\ldots + V_n^2}}{V_1^2} \times 100$$

Where:

- V_1 is the amplitude of the fundamental frequency (grid frequency, e.g., 50 Hz).
- $V_2, V_3, \ldots, V_n$ are the amplitudes of higher harmonic components.

This calculation helps quantify the impact of the harmonics generated by the VSC and other system components like the boost converter and nonlinear loads.

Role of THD Minimization

1. Improved Power Quality:
   - Reducing THD ensures that the grid current remains clean and free from excessive harmonic distortion, improving the overall power quality delivered to the grid.
2. Harmonic Mitigation by Passive Filter:
   - A passive filter with a resistance of 1.25 kΩ and capacitance of 125 nF is employed in the system to suppress harmonics introduced by the switching operation of the VSC. This helps in achieving lower THD values.
3. Fuzzy Logic Control in VSC:
   - The Mamdani Fuzzy Inference System used for VSC control plays a vital role in reducing THD. By dynamically modifying the grid current to modify the switching pulses error and its rate of change, the controller ensures smoother waveforms and minimizes harmonic distortion.
4. Compliance with Grid Standards:
   - By maintaining a low THD value, the system adheres to grid codes and standards for harmonic distortion, ensuring stable and efficient operation of the grid-connected PV system.

6. RESULTS & DISCUSSION

6.1 ANN Controller in MPPT & Adaptive Controller in VSC

The Figure. 4(a) demonstrates the system response when the ANN controller is applied for MPPT and the adaptive controller is used in the VSC. Under abnormal grid anomalies, the grid voltages (V_{sabc}) are effectively maintained, ensuring balance and sinusoidal behaviour even under linear and non-linear load circumstances.

Figure 4(a) Results of a solar energy transition system simulation with ANN & Adaptive Control Configuration.

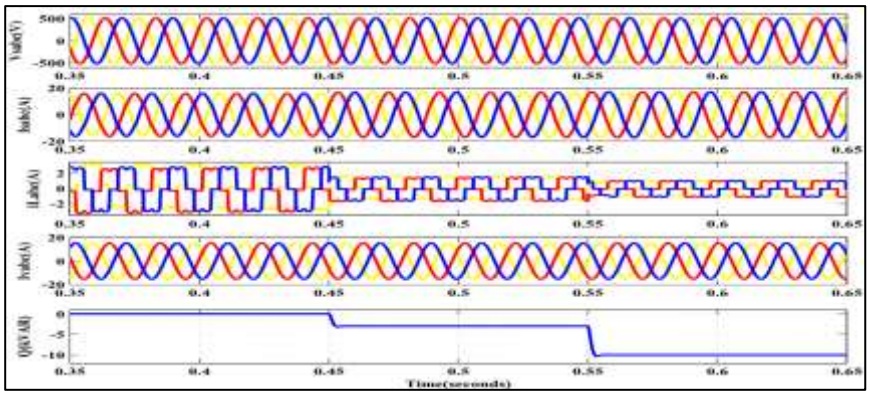

The Isabc grid currents are sinusoidal and balanced. showing reduced harmonic content and proper alignment with the grid voltages. The load currents (i_{Labc}) exhibit stable operation with minor transients during disturbances, ensuring a reliable supply to the load. The VSC currents (I_{vabc}) adaptively regulate the dynamic changes, stabilizing quickly and maintaining the required current profile for proper power injection. The system

provides supporting reactive power for voltage stability in accordance with IEEE 1547 grid code. The power factor (Q) achieves near-unity operation shortly after the transient period, demonstrating efficient operation and minimal reactive power exchange with the grid.

Figure 4(b) Simulated results of SECS with V_{dc}, I_{pv}, P_{pv}, I^*_{sa}-I_{sa} .

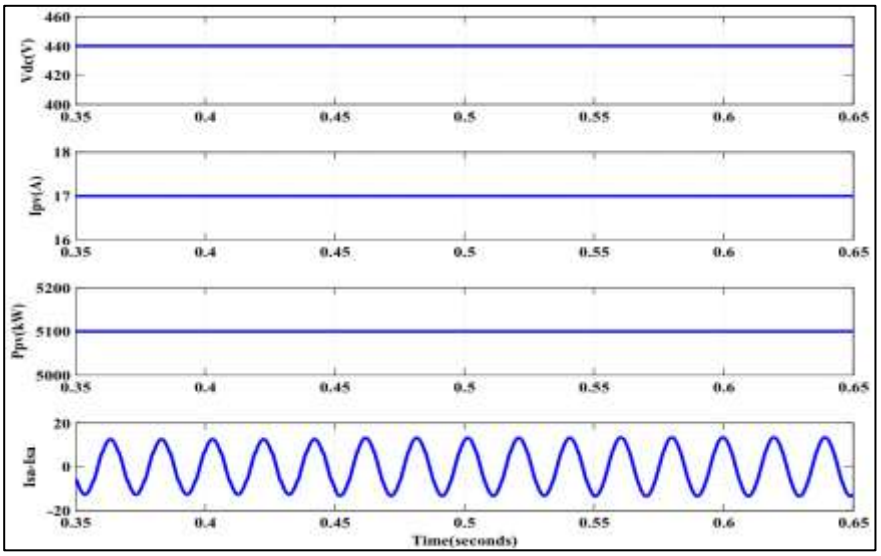

From Figure. 4(b), the DC bus voltage (V_{dc}) remains stable, indicating effective regulation and proper functioning of the DC connection. The PV current (I_{pv}) and PV power (P_{pv}) are consistent, which reflects the steady and efficient performance of the photovoltaic system. This steady current and power output suggest that The system is functioning in ideal circumstances. without any disruptions. The I^*_{sa}-I_{sa} waveform displays smooth sinusoidal oscillations, indicating effective current regulation and stability. The clean waveform highlights that the current remains well-tracked and controlled within the desired limits, ensuring reliable and smooth functioning of the entire system.

6.2 ANN Controller in MPPT & Fuzzy Logic Controller in VSC

The Figure. 5(a) illustrates the system response when the ANN controller is utilized for MPPT and the fuzzy logic controller governs the VSC. Despite the abnormal grid anomalies, the grid voltages (V_{sabc}) are successfully maintained, remaining balanced and sinusoidal under linear and non-linear load conditions, highlighting proper voltage regulation and grid synchronization. In sync with the voltages, the grid voltages (I_{sabc}) exhibit sinusoidal behavior. showing minimal harmonic distortions and efficient operation. The load currents (I_{Labc}) are stable and sinusoidal, with no significant distortions during steady-state and transient periods, ensuring uninterrupted and high- quality power delivery to the load. The VSC currents (I_{vabc}) demonstrate precise and consistent regulation, adapting effectively to dynamic conditions without introducing oscillations, thanks to the fuzzy logic controller's handling of nonlinearities. The power factor (Q) remains consistently close to unity, ensuring optimal operation and efficient reactive power compensation in compliance with IEEE 1547 standards. As observed in Figure. 5(b) The DC bus voltage (V_{dc}) remains constant, demonstrating stable voltage regulation and reliable system operation. The PV current (I_{pv}) and PV power (P_{pv}) also remain steady, reflecting consistent and efficient power delivery from the photovoltaic source. This shows that the system operates efficiently under the given conditions without any significant fluctuations. The I^*_{sa}-I_{sa} waveform exhibits a clean sinusoidal pattern, representing smooth current regulation and proper system behaviour. The overall stability of the current waveform suggests that the system maintains accuracy and performs without distortions or irregularities, ensuring smooth and reliable performance.

Figure 5(a) Simulated results of solar energy conversion system with ANN & Fuzzy Logic Control Configuration.

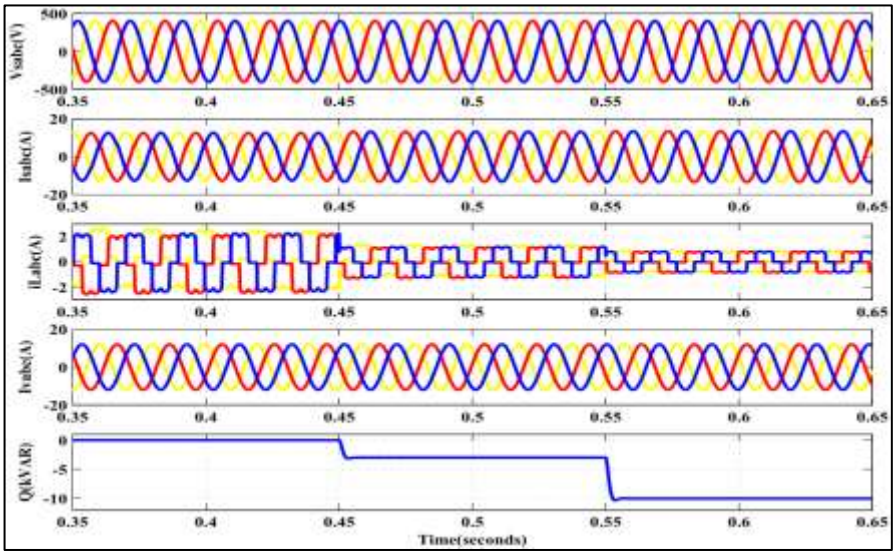

Figure 5(b) Simulated results of SECS with V_{dc}, I_{pv}, P_{pv}, I^{*}_{sa}-I_{sa} .

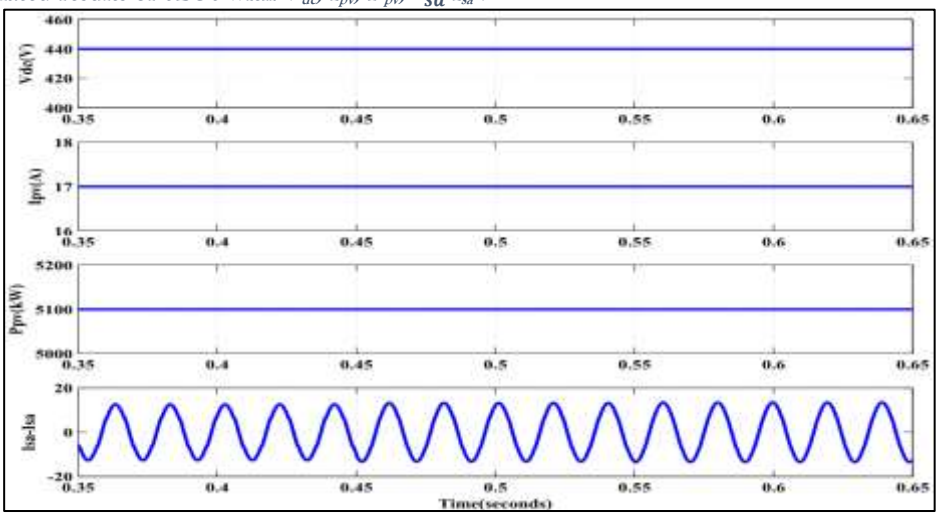

7. COMPARITIVE RESULTS

The presented work focuses on the performance analysis of an ANN Controller in MPPT and VSC systems controlled with Fuzzy Logic Control for reducing voltage and current total harmonic distortion (THD), ensuring compliance with international standards.

Figure 6(a) THD% observation of Grid Voltage under ANN & Adaptive Control Configuration.

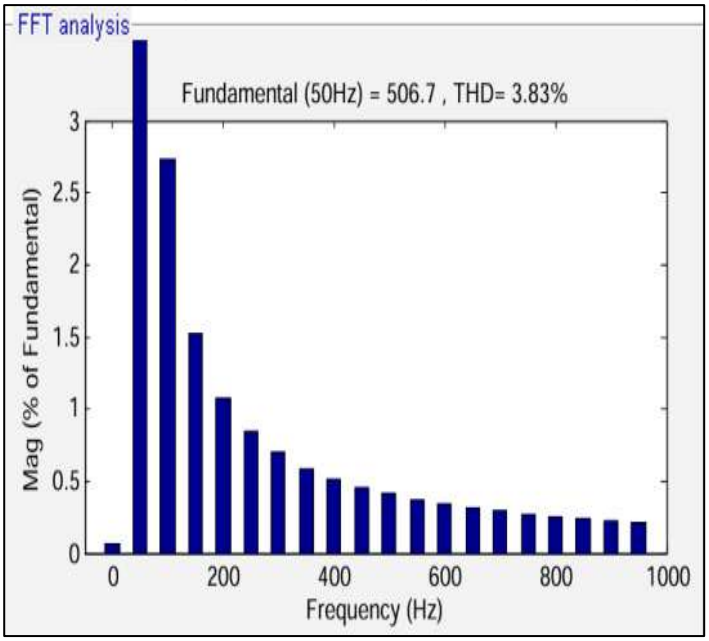

Figure 6(b) THD% observation of Grid Current under ANN & Adaptive Control Configuration.

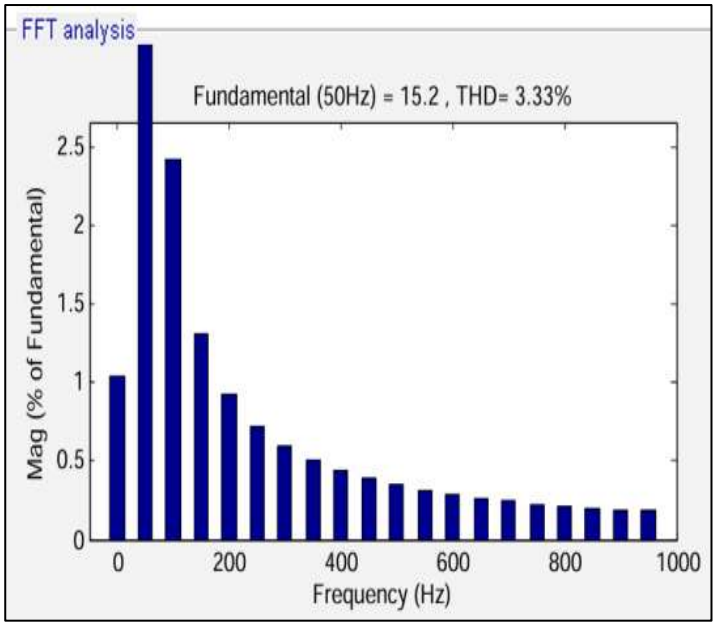

Figure 7(a) THD% observation of Grid Voltage under ANN & Fuzzy Logic Control Configuration.

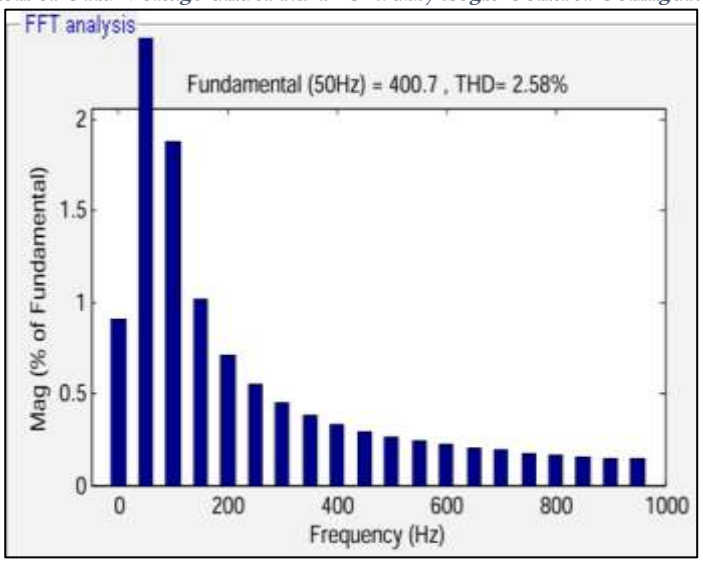

Figure 7(b) THD% observation of Grid Current under ANN & Fuzzy Logic Control Configuration.

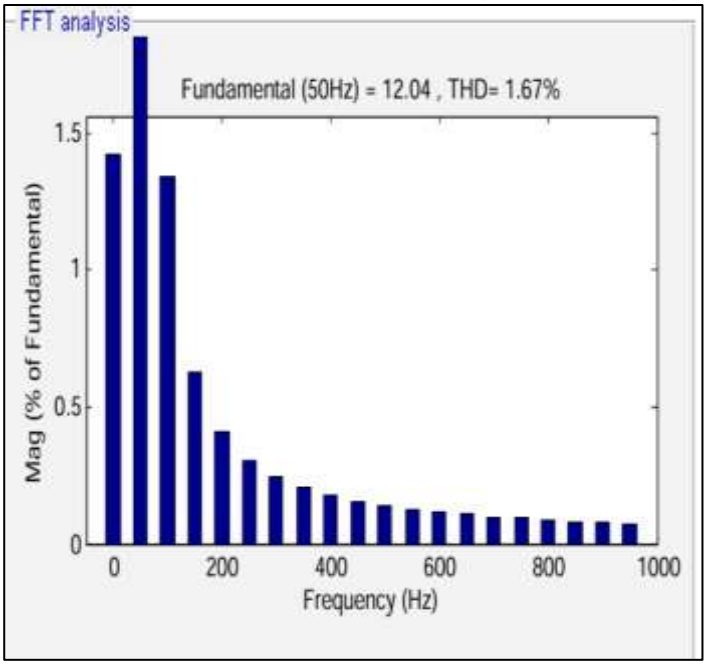

The study highlights two configurations of the ANN-based fuzzy logic control system, where the first configuration achieves a Voltage THD of 3.83% and a Current THD of 3.33%, both well within the permissible limits set by

IEEE 519 and IEC 61727 standards, which recommend a THD limit of ≤ 5%. The second configuration demonstrates even better performance, achieving a Voltage THD of 2.58% and a Current THD of 1.67%, indicating a significant improvement in harmonic suppression. This enhanced performance ensures minimal grid disturbances, improved power quality, and superior system stability. The work underscores how well MPPT and VSC systems' harmonic performance may be optimized using an ANN-based fuzzy logic controller, offering a robust and efficient solution for maintaining power quality standards. Such results demonstrate the potential of advanced control strategies like ANN and fuzzy logic in achieving precise and adaptive control for renewable energy systems, making them highly suitable for grid-connected applications where maintaining harmonic quality is crucial.

Table 2 THD Comparision Table

Parameter	ANN Controller in MPPT&VSC Controlled with Adaptive Controller	ANN Controller in MPPT&VSC Controlled with Fuzzy Logic Controller
Grid Voltage	3.83%	2.58%
Grid Current	3.33%	1.67%

8. CONCLUSION

The simulation results further illustrate that integrating ANN controllers for MPPT with advanced control techniques, such as adaptive and fuzzy logic controllers in VSCs, significantly enhances the performance and reliability of grid-connected PV systems. The ANN and fuzzy logic controller configuration achieved superior harmonic suppression, with a Voltage THD of 2.58% and a Current THD of 1.67%, showcasing its effectiveness in minimizing harmonic distortions and ensuring compliance with international standards. The system's ability to maintain balanced and sinusoidal grid voltages and currents, even under non-linear load conditions and grid anomalies, highlights its adaptability and robustness. Stable DC bus voltage, near-unity power factor operation, and precise regulation of PV current and power further confirm the system's efficient energy conversion and grid integration. The clean and well-regulated current waveforms reflect the accuracy and reliability of the proposed control strategies in dynamic operating scenarios. These results underscore the advantages of combining ANN-based MPPT with adaptive and fuzzy logic controllers in VSCs for delivering high power quality and efficient performance. This approach demonstrates a promising direction for developing advanced grid-connected PV systems that ensure seamless operation and compliance with stringent power quality standards.

REFERENCES

[1] Priyank Shah and Xiaowei Zhao, "Using a passive filter to mitigate leakage current in solar power plants array systems," Energy Conversion IEEE Trans. vol. 38, no. 1, March 2023.

[2] A. Molina-Garcia, J. Guerrero-Pérez, M. C. Bueso, M. Kessler, and E. Gómez-Lázaro, "A new symmetrical and shifted Gompertz model-based solar panel modeling for photovoltaic applications, IEEE Trans. Energy Conv., vol. 30, no. 1, pp. 51–59, Mar. 2015.

[3] Bikash sah, Praveen Kumar, Sanjay Kumar Bose, IEEE SYSTEMS JOURNAL, "A Vehicle-to-Grid System Intelligent Controller Based on Fuzzy Logic and Synthetic Neural Networks," July 2020.

[4] V. L. Srinivas, B. Singh, and S. Mishra"Enhanced power quality PV-inverter for three-phase SECS with suppression of leakage current," IEEE Electron. Trans. Ind. vol. 69, no. 6, pp. 5756–5767, Jun. 2022.

[5] L. Qian, D. A. Cartes, and H. Li, "An enhanced adaptive detection technique to enhance power quality," *IEEE Trans. Ind. Appl.*, vol. 44, no. 2, pp. 525–533, Mar./Apr. 2008.

[6] R. A. Freeman and P. Kokotovic´, Modern Birkhäuser Classics Book Series (MBC), Sturdy Nonlinear Control Mechanism. Boston, MA, USA: Birkhauser, 1996.

[7] R. Panigrahi, S. K. Mishra, S. C. Srivastava, A. K. Srivastava, and N. N. Schulz, "Review of small-scale solar systems' grid integration in secondary distribution networks Trans. Ind. Appl. IEEE, vol. 56, no. 3, pp. 3178–3195, May/Jun. 2020.

[8] Low-voltage distribution network-connected power production systems—Technical prerequisites for connecting to and operating in parallel with these networks, VDE-ARN 4105-2011, 2011.

[9] M. Rabiul Islam, A. M. Mahfuz-Ur-Rahman, K. M. Muttaqi, and D. Sutanto, "State-of-the-art of the medium-voltage power con- verter technologies for grid integration of solar photovoltaic power plants," *IEEE Trans. Energy Convers.*, vol. 34, no. 1, pp. 372–384, Mar. 2019.

[10] M. N. H. Khan, M. Forouzesh, Y. P. Siwakoti, L. Li, T. Kerekes, and F. Blaabjerg, "A comparative review of transformer-less converter topologies for single-phase photovoltaic systems," IEEE Trans. *Emerg. Sel. Topics Power Electron.*, vol. 8, no. 1, pp. 805–835, Mar. 2020.

[11] W. Wu, Y. Sun, Z. Lin, T. Tang, F. Blaabjerg, and H. Shu-Hung Chung, "A novel LCL-filter for a single-phase grid-tied inverter with an in-series parallel resonant circuit," *IEEE Trans. Ind. Electron.*, vol. 61, no. 9, pp. 4640–4644, Sep. 2014.

[12] R. Morfin-Magaña, J. J. Rico-Melgoza, F. Ornelas-Tellez, and F. Vasca, "A photovoltaic power electronic system's complementarity model with model predictive control," *IEEE Trans. Circuits Syst. I: Regular Papers*, vol. 66, no. 11, pp. 4402–4414, Nov. 2019.

[13] L. B. G. Campanhol, S. A. O. da Silva, A. A. de Oliveira, and V. Dário Bacon"Analysis of power flow and stability in a multipurpose distributed generation system that integrates a photovoltaic system with a unified power quality conditioner," *IEEE Trans. Power Electron.*, vol. 34, no. 7, pp. 6241–6256, Jul. 2019.
[14] M. M. Swamy and M. A. Baumgardner, "New dv/dt filter in normal mode with an integrated resistor failure detection circuit," *IEEE Trans. Ind. Appl.*, vol. 53, no. 3, pp. 2149–2158, May/Jun. 2017.
[15] R. Ruffo, P. Guglielmi, and E. Armando"Inverter side RL filter with precise design for reducing motor overvoltage in SiC-based drives," *IEEE Trans. Ind. Electron.*, vol. 67, no. 2, pp. 863–873, Feb. 2020.
[16] J. Xu, J. Han, Y. Wang, S. Habib, and H. Tang, "A new scalar PWM technique to lower leakage current in transformer-less grid-connected VSIs with three phases and two levels," *IEEE Trans. Ind. Electron.*, vol. 67, no. 5, pp. 3788–3797, May 2020.
[17] S. Jeong, D. Shin, and J. Kim, "A common-mode active EMI filter isolated by a transformer that doesn't require any extra parts on power lines," *IEEE Trans. Power Electron.*, vol. 34, no. 3, pp. 2244–2257, Mar. 2019.
[18] J. C. Giacomini, L. Michels, H. Pinheiro, and C. Rech, "Active dampening technique for transformer-less, three-phase, grid-connected photovoltaic inverters to reduce leakage current," *IEEE Trans. Power Electron.*, vol. 33, no. 5, pp. 3988–3999, May 2018.
[19] M. Taul, "Synchronization stability of grid-connected converters under grid faults," Ph.D. dissertation, Faculty Eng. Sci., Aalborg, Denmark: Aalborg Univ., pp. 1–120, 2020.
[20] D. Sera, L. Mathe, T. Kerekes, S. V. Spataru, and R. Teodorescu, "On the perturb-and-observe and incremental conductance MPPT methods for PV systems," *IEEE J. Photovolt.*, vol. 3, no. 3, pp. 1070–1078, Jul. 2013.
[21] W. Libo, Z. Zhengming, and L. Jianzheng, "A single-stage three-phase grid-connected photovoltaic system with modified MPPT method and reactive power compensation," *IEEE Trans. Energy Convers.*, vol. 22, no. 4, pp. 881–886, Dec. 2007.
[22] T. Chang, K. Lo, and C.-T. Pan, "A novel vector control hysteresis current controller for induction motor drives," *IEEE Trans. Energy Convers.*, vol. 9, no. 2, pp. 297–303, Jun. 1994.
[23] S. Dhara and V. T. Somasekhar, "A three-phase semi-single stage PV inverter with voltage boosting and leakage current minimization," *IEEE Trans. Circuits Syst. II: Exp. Briefs*, vol. 69, no. 1, pp. 169–173, Jan. 2022.
[24] J. Jiang, S. Pan, J. Gong, F. Liu, X. Zha, and Y. Zhuang, "A leakage current eliminated and power oscillation suppressed single-phase single- stage non-isolated photovoltaic grid-tied inverter and its improved control strategy," *IEEE Trans. Power Electron.*, vol. 36, no. 6, pp. 6738–6749, Jun. 2021.
[25] X. Guo, Y. Yang, R. He, B. Wang, and F. Blaabjerg, "Transformer-less Z-source four-leg PV inverter with leakage current reduction," *IEEE Trans. Power Electron.*, vol. 34, no. 5, pp. 4343–4352, May 2019.
[26] L. Qian, "*A New Adaptive Detection Algorithm For Power Qual- ity Improvement*". Tallahassee. FL, USA: Florida State Univ., Sep. 2007.
[27] M. Karimi-Ghartemani, S. A. Khajehoddin, P. Jain, and A. Bakhshai, "A systematic approach to DC-bus control design in single-phase grid- connected renewable converters," *IEEE Trans. Power Electron.*, vol. 28, no. 7, pp. 3158–3166, Jul. 2013.